THE JOURNAL OF PHYSICAL CHEMISTRY B

Article

pubs.acs.org/JPCB

Dynamics of Water/Methanol Mixtures at Functionalized Chromatographic Interfaces

Prashant Kumar Gupta and Markus Meuwly*

Department of Chemistry, University of Basel, Klingelbergstrasse 80, 4056 Basel, Switzerland

Supporting Information

ABSTRACT: Fully atomistic simulations of water/methanol mixtures of varying compositions (80/20 and 50/50) at chromatographic interfaces with different functionalizations are presented. The dynamical properties in terms of equilibration times and solvent exchange dynamics are characterized and found to depend on the different systems on the nanosecond time scale. The solvent density profile and the structuring of the stationary phase differ for derivatizations including (−CN, NO_2, $-NH_2$, $-C_6H_5$) of the C_{18} chain. The time scale and intensity of the water exchange dynamics differs for the different realizations of the chromatographic systems and ranges from 200 to 500 ps. Water exchange rates depend on solvent composition as well as on the functionalization of alkyl chains. Simulations with acridine as a probe molecule provide atomistic insight into the slot model.

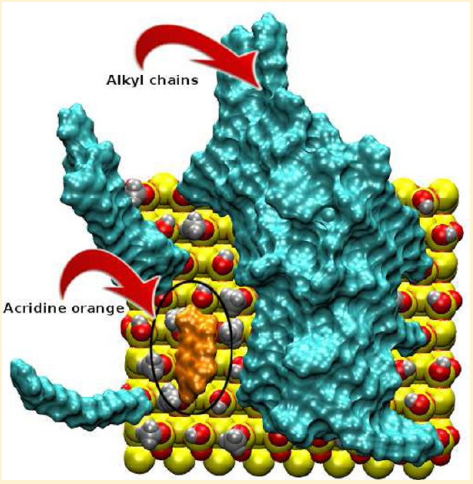

I. INTRODUCTION

Reversed-phase liquid chromatography (RPLC) is a technologically important method in analytical chemistry. Despite the seemingly "simple" chemical composition of such systems (functionalized silica surface, solvent mixture, and analyte molecules), the atomistic understanding underlying the separation process remains elusive. One of the reasons for this is that the systems of interest are intrinsically disordered which makes controlled and atomistically resolved experiments difficult. Furthermore, the systems are highly dynamical which adds to the complexity. Under such circumstances, computational methods are an ideal means to obtain additional insights and have considerably contributed to better characterize such systems.[1−14]

Typically, a chromatographic system contains an alkyl-chain-derivatized stationary phase, a solvent mixture, and analyte molecules. All these components interact through nonbonded interactions and are subject to intermolecular dynamics. The nature and composition of the mobile phase, together with the functionalization of the stationary phase, play a decisive role in the separation process. Commonly used solvent mixtures include water (H_2O) and an organic cosolvent such as acetonitrile (ACN) or methanol (MeOH). The composition of the solvent is adjusted to change the hydrophobic character of the solution and affects the elution time for the analyte. Water provides strong polar interactions, whereas addition of the organic cosolvent controls the hydrophobic character of the solution and leads to microheterogeneity.

Experimentally, spectroscopy methods including IR,[15−17] Raman,[18] and NMR[19−21] investigations have provided detailed information about water/methanol mixtures. However, because the systems are highly dynamical, molecular-level information is difficult to obtain. The general consensus is that such solutions separate into MeOH-rich regions and water-rich regions and lead to microheterogeneous[2,8,22,23] or microimmiscible[24−26] solutions at microscopic levels which was also observed experimentally by Raman spectroscopy for water/acetonitrile mixtures.[27] Given the different polarities of ACN (CH_3CN) and MeOH (CH_3OH) and the hydrogen-bonding capabilities of MeOH, the structure and dynamics of ACN/water and MeOH/water mixtures at a chromatographic interface can be expected to be quite different. In chromatographic systems the derivatization of the stationary phase is another important determinant.[28] The alkyl chains are nonpolar whereas the surface to which they are attached is polar.

Atomistic simulations have provided detailed information about structural features and morphologies of the surfaces. Most recently, the solvent distribution C_{18} stationary phases was characterized for different ACN/water and MeOH/water mixtures from configurational-bias Monte Carlo simulations.[29] While such simulations are useful to obtain thermodynamic information, including the distribution of the solvent at the interface, they are less suitable to follow the intermolecular

Received: June 1, 2012
Revised: July 17, 2012
Published: July 27, 2012

dynamics for which molecular dynamics (MD) simulations are the preferred technology.[1−3,8,10] Given that chromatographic systems are highly dynamical, directly monitoring the intermolecular dynamics, including the exchange dynamics at the interface, is of fundamental interest.

In the present work the primary focus is on the solvent distribution and exchange dynamics at unfunctionalized and functionalized stationary phases with different MeOH/water mixtures. It is found that the morphology of the solvent phase closely reflects that from MC simulations. The exchange dynamics on the nanosecond time scale depends on both the functionalization and the solvent mixture. Finally, the behavior of an analyte—acridine orange—at the surface was also considered for different conditions.

II. THEORETICAL AND COMPUTATIONAL METHODS

A. Description of the Chromatographic Column. A model silica support was constructed by slicing two 8.75 Å thick segments of the (101) face of quartz crystalline lattice with dimensions of 36 × 41 Å. This resulted in two −OH-terminated surfaces with a vicinal silanol density of 3.1 μmol/m^2. A chromatography column was then created by covalently tethering alkylsilane ligands (with alkyl chains in an all trans conformation) to the silanol oxygen atoms of the quartz surface and orthogonal to the bulk quartz. Alkyl chains were evenly distributed over the surface silanols in a randomized fashion to result in a specific surface coverage of 0.88 and 2.65 μmol/m^2. A 80 Å thick solvent box (water/methanol) was added between the two silica surfaces, resulting in a unit cell with dimensions of 36 × 41 × 97 Å. The simulation system is shown in Figure 1.

In the present work, the transferable intermolecular potential three-point (TIP3P)[30] water model was used. For the methanol (MeOH) molecule, methyl hydrogen atoms were assigned to aliphatic hydrogen (atom type HA), the methyl-C atom is an aliphatic SP3 carbon (CT3), the hydroxyl oxygen is a polar oxygen (OH1), and the hydroxy hydrogen atom was assigned to a polar hydrogen (H).[31] The OH equilibrium bond length is 0.96 Å.[31] The MeOH is flexible with standard CHARMM parameters used for the CT3−OH1 bond, the HA−CT3−OH1 and HA−OH1−CT3 angles, and the dihedrals.[31] As for water, SHAKE[32] was used to constrain all hydrogen atoms.

Five different functionalizations of the chromatographic column are considered and studied here with two different solvent compositions. The functionalizations include $-CH_3$, $-CN$, $-NH_2$, $-NO_2$, and $-C_6H_5$, and their parametrization has been reported in earlier work.[10] Briefly, for $-CN$, $-NH_2$, and $-C_6H_5$ existing CHARMM parameters[31] were employed in analogy to lysine and phenylalanine. For $-NO_2$ literature values[33] were used. Details concerning the number of molecules (water and methanol) and the solvent composition are reported in Table 1. Labels such as C17phenyl.20.80 in Table 1 refer to a silica surface containing C17-chain with a −phenyl functionalization and a W/MeOH solvent composition of 80/20 volume fractions. "Low" and "high" correspond to 0.88 and 2.65 μmol/m^2 surface coverage of the functionalized chains. The force field parameters for the Si−O and O−C bonds ($V = {}^1/_2k(r - r_e)^2$) were (k = 525.0 kcal/mol, r_e = 1.62 Å) and (k = 428.0 kcal/mol, r_e = 1.42 Å), respectively; for the Si−O−C, O−Si−O, and O−C−C angles ($V = {}^1/_2k(\theta - \theta_e)^2$) were ($k$ = 40.0 kcal/mol, θ_e = 120.0°), (k = 40.0 kcal/mol, θ_e = 90.0°), (k = 40.0 kcal/mol, θ_e = 110.0°), respectively; and for the Si−O−C−C and O−C−C−C dihedral angles ($V = k(1+\cos[n\chi - \delta])$) they were ($k$ = 0.15 kcal/mol, n = 1, δ = 0.0°). The −OH groups bonded to the Si layer had point charges of +0.66e and −0.66e for hydrogen and oxygen atoms, respectively.

For acridine orange, the force field parameters are those previously reported.[8]

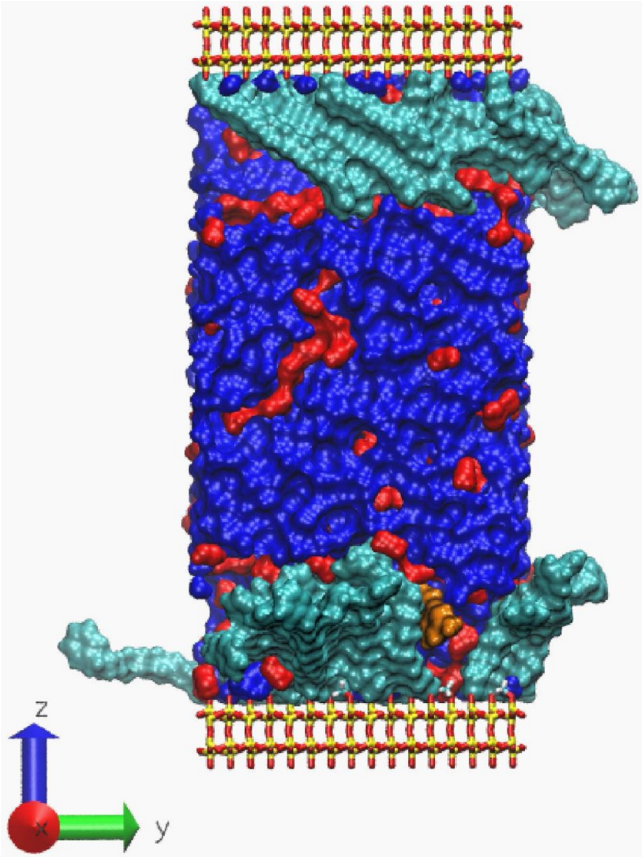

Figure 1. Schematic representation of the chromatographic system along with the analyte molecule. The figure shows the silica layer (silica in yellow, oxygen in red), C_{17}-phenyl chains (green) grafted onto it, water (blue), methanol (red), and acridine orange (orange). The snapshot is taken during the simulation of acridine orange in C_{17}-phenyl functionalized system with 80/20 W/MeOH solvent concentration.

Table 1. Number of W/MeOH Molecules for Different Simulations and Solvent Mixtures, 80/20 and 50/50 Volume Fraction, Respectively[a]

	surface coverage	
systems	low	high
C18.20.80	2985/343	2518/280
C18.50.50	1710/640	1456/524
C17cn.20.80	3072/336	2466/292
C17cn.50.50	1731/632	1609/576
C18nh2.20.80	3042/271	2804/244
C18nh2.50.50	1814/692	1609/571
C18no2.20.80	2891/272	2777/255
C18no2.50.50	1783/625	1642/598
C17phenyl.20.80	2975/275	2273/220
C17phenyl.50.50	1783/690	1572/544

[a]Low and high correspond to the surface coverage 0.88 and 2.65 μmol/m^2.

dx.doi.org/10.1021/jp305351f | J. Phys. Chem. B 2012, 116, 10951−10959

B. Molecular Dynamics Simulations. For all molecular dynamics (MD) simulations the same protocol was used. After solvation, the systems were subjected to 500 steps of steepest descent minimization followed by 200 steps with the Adopted Basis Newton−Raphson algorithm to relieve strain. Next, MD simulations were carried out at constant volume and constant temperature (*NVT*) using the CHARMM program.[34] The time step in all simulations was 1 fs, and SHAKE[32] was used to constrain the bonds to hydrogen atoms. All simulations were carried out with periodic boundary conditions. Nonbonded interactions were truncated at a distance of 10 Å on an atom-by-atom basis, using a shift function for the electrostatic interactions and a switch algorithm for the van der Waals interactions.[35] The atomic positions of the bulk quartz surface with the exception of the exposed hydrogen atoms of the silanol groups were held fixed during the simulation (1664 atoms). Initially, the systems were heated and equilibrated for 50 ps, followed by 2 ns of production simulations. Atomic coordinates from the MD simulations were recorded at 50 fs intervals for analysis. For every system with different functionalizations one simulation was carried out, except for C18 alkyl chains, for which five independent simulations were run.

Apart from the above setup, the dynamics of acridine orange in a ($-C_6H_5$) derivatized alkyl column was investigated. An analyte molecule (acridine orange) was introduced into an equilibrated C_{17}-phenyl column. Water molecules overlapping with the analyte molecule were removed, and then production simulations were continued for 5 ns to study the dynamics of the analyte. These simulations were run in the C_{17}-phenyl system with high surface coverage (2.65 μmol/m^2) in solvent mixtures W/MeOH (100/0, 80/20 and 50/50) for both protonated (NH^+) and unprotonated (N) acridine.

C. Analysis of the Trajectories. Observables to characterize the chromatographic systems were determined from ensemble averages. They include the alkylsilane chain length, solvent density, acridine position with respect to the silica surface, and the diffusion coefficient of the analyte (acridine orange), which is calculated from the Einstein relation[36]

$$D = \frac{\langle |\vec{r}_i(t) - \vec{r}_i(0)|^2 \rangle}{6t} \quad (1)$$

where $\vec{r}_i(t)$ is the position of the center of mass of a single molecule.

Previous experimental[37] and simulation studies[38] suggested that a typical chromatographic system with a C18 stationary phase can be largely decomposed into three different types of water molecules. In order to analyze the water dynamics, three separate regions are considered: region I, defined as water molecules within 2.4 Å of Si-bonded oxygen atoms, referred to as "bonded water molecules"; region II, defined as water molecules within 18 Å of the silica layer, called "stationary"; and region III, defined as water molecules between 20 and 60 Å away from the surface are called "bulk" water. Depending upon the initial position, water molecules are either in regions I, II, or III. The number of water molecules that left a specific region during the production phase and entered a neighboring region is used to follow equilibration of the systems. Another useful observable is the width of the stationary phase $\langle z \rangle$, which is referred to as the "phase thickness". It is defined as the average vertical distance of the terminal carbon atom of the alkyl chains farthest away from the silica support.

III. RESULTS

A. Solvent Mixture without Alkyl Chains. First, the behavior of the solvent mixture is studied for the unfunctionalized systems but with the silica support which defines $z = 0$ and $z = 80$ Å. The density of the solvent along the z-axis (along the height of the column) is shown in Figure 2 for W/MeOH

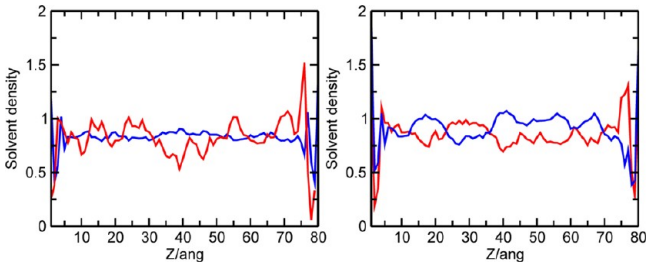

Figure 2. Solvent density profile for 80/20 (left) and 50/50 (right) volume fraction of solvent mixture without the presence of any functionalized chain on the silica layer.

mixtures of 80/20 and 50/50 volume fraction, respectively. The density ρ of the solvent

$$\rho = \frac{n_s}{n_s^{id}} \quad (2)$$

is calculated from the number of solvent molecules (water or MeOH) in a slab of 1 Å width relative to the number of solvent molecules in the same slab for an ideal, homogeneous mixture. The density of the solvent molecules in Figure 2 is averaged over the last 100 ps from 1900 to 2000 ps. For both mixtures away from the surface a local high density of one component is balanced by a low density of the other component. This is typical of microheterogeneity at a microscopic level in which self-association of the same type of molecule is found[8,29] with continuous microheterogeneity proposed by Reimers and Hall.[27] The variation of the density profiles across the column depends on the relative concentrations of the solvent mixture. This agrees qualitatively with neutron diffraction experiments which found that methanol and water form percolating networks in which water molecule form clusters of typical sizes ranging from 2 to 20 (see also Figure 1).[39,40] Similar effects were recently observed in wide- and small-angle neutron scattering experiments on sorbitol−water mixtures.[41]

B. Characterization of the Solvent Mixtures. Depending on solvent composition, surface density, and functionalization of the alkyl chains, different organization of the solvent in and close to the surface of the stationary phase can be expected. With both solvent compositions (80/20 and 50/50), both surface coverages (2.65 and 0.88 μmol/m^2) and all functionalizations, the solvent density deviates from a uniform distribution $\rho = 1$. Rather, both water and MeOH densities decrease when approaching the stationary phase from the middle of the column ($z = 40$ Å). This is shown in Figure 3 (for C_{18} and C_{17}-phenyl) and Figures S1 and S2 (for C_{17}−CN, C_{18}−NH_2, C_{18}−NO_2) in the Supporting Information. Between the stationary phases, which differ in their width depending on the system (see Table 2), microheterogeneity is still observed. Furthermore, common to all preparations of the systems is a more or less pronounced MeOH density about 5 Å away from the surface and a preserved water density at the surface. In other words, the silica (Si−OH) surface is "wet" and hydrated.

dx.doi.org/10.1021/jp305351f | J. Phys. Chem. B 2012, 116, 10951−10959

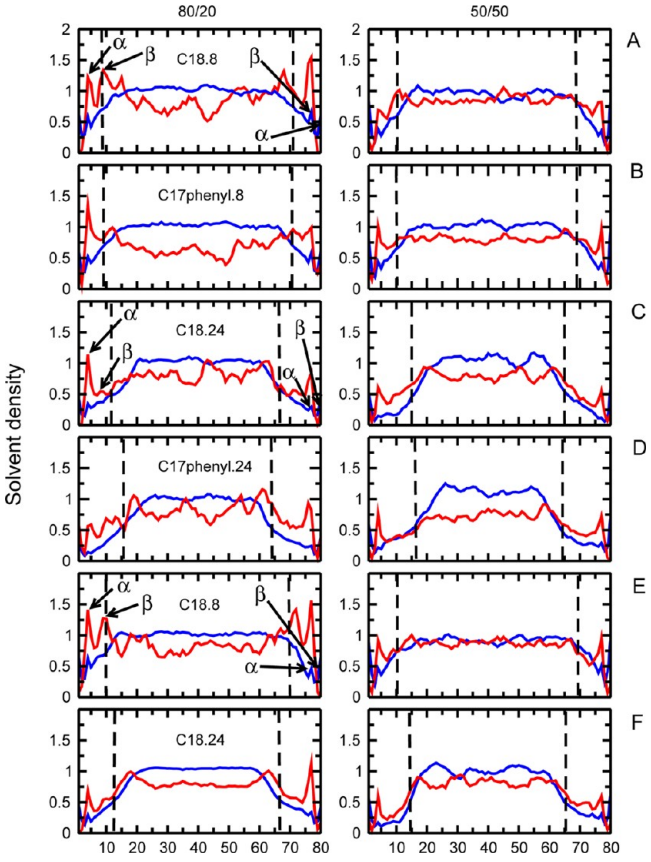

Figure 3. Average solvent density profile (over 100 ps from 1900 to 2000 ps of simulation time) with C_{18} and C_{17}-phenyl chains and 80/20 W/MeOH solvent composition (left) and 50/50 W/MeOH composition (right). (A: unfunctionalized C_{18} low coverage; B: C_{17}-phenyl low coverage; C: C_{18} high coverage; D: C_{17}-phenyl high coverage; E: C_{18} low coverage average over 4 independent simulations; F: C_{18} high coverage average over 4 independent simulations. Blue traces correspond to water density, and red traces correspond to MeOH density. The *y*-axis gives the density of the solvent as defined in eq 2.

Table 2. Functionalized Alkyl Chain Phase Thickness $\langle z \rangle$ Measured in Å, Defined as the Average Height of the Functionalized Alkyl Chains Relative to the Silica Layer[a]

$\langle z \rangle$	methanol		acetonitrile		N_{water}
system	low	high	low	high	high
C18.20.80	8.9	13.1	8.0	13.2	35(1)
C18.50.50	10.7	14.8	12.1	15.2	30(1)
C17cn.20.80	10.2	15.3	9.2	13.5	36(1)
C17cn.50.50	11.1	16.8	11.6	16.5	32(1)
C18nh2.20.80	8.2	16.6	9.8	11.8	30(1)
C18nh2.50.50	12.7	13.5	12.8	15.2	25(1)
C18no2.20.80	8.6	14.5	10.0	14.1	37(1)
C18no2.50.50	10.6	15.9	11.1	16.1	33(1)
C17phenyl.20.80	9.2	15.3	9.3	15.4	34(1)
C17phenyl.50.50	10.6	16.6	16.7	14.3	32(1)

[a]Data are compared with previous work for acetonitrile as a cosolvent. These data are calculated as averages over 2 ns of MD simulation. Low and high refer to the surface coverage.

This agrees with previous work for acetonitrile/water and pure water solvent.[8,29,38]

Comparing low (Figure 3A,B) and high (Figure 3C,D) coverage surfaces, it is observed that the width over which the water distributes is ∼5 Å wider for low alkyl chain coverage. This, together with the analysis in Table 2, suggests that the alkyl chains are in a more collapsed state for low surface coverage. With high surface coverage, the alkyl chains are forced into a more parallel conformation which leads to increased conformational stability and a more upright and brushlike arrangement. Similar behavior is found for the other functionalizations (see Figures S1 and S2).

Increased MeOH concentrations (50/50 compared to 80/20) change ρ_{MeOH} in the middle of the column. In general, fluctuations in ρ_{MeOH} are more pronounced for 80/20 compared to 50/50 solvent composition. This is due to increased MeOH concentration in the solvent (Figures 3A,B and 3C,D). The density maxima in ρ_{MeOH} within ≈5 Å of the surface are more pronounced for low methanol concentration and for both low and high surface coverage and are indicated by α and β labels in Figure 3. These peaks are due to MeOH close to the surface forming a transient layered structure. For a 50/50 solvent composition these peaks are not sharp because as the MeOH concentration increases, it is more homogeneously distributed in the solvent mixture which leads to a decrease in the microheterogeneous structure compared to 80/20 solvent composition. This also shows that microheterogeneity is concentration-dependent and continuous.[27] Comparison of the different functionalization shows that the widths of the stationary phases can vary by 10−25% (see Table 2), depending on the terminal group attached to the chain and the solvent composition.

In order to determine how representative individual trajectories are to characterize the different systems, four independent simulations were run for high- and low-surface coverage C18 with W/MeOH mixtures of 80/20 and 50/50, respectively. Figures 3E,F report average density distributions from four independent simulations. The density distribution is similar to what is found from individual trajectories (see Figures 3A,C), which suggests that the current simulations cover most of the important parts of phase space.

In all systems studied, an appreciable amount of water is found at the surface which corresponds to H-bonded water molecules (Figures 3). However, the precise amount also depends on solvent concentration and surface coverage (see Table 2). As the MeOH volume fraction in the mixture increases, the number of water molecules close to the surface reduces. With increasing surface coverage of the stationary phase the hydrophobic interaction increases. This is another reason for the decrease in the water density at the surface. Table 2 shows that for given surface coverage the number of water molecules for most functionalizations increases by ≈15%, whereas it is only 6% for C_{17}-phenyl chains.[29]

In order to better understand the double ρ_{MeOH} peak α and β within 10 Å of the silica surface, as observed for most systems studied (Figure 3), the orientation of the methanol−OH bond vector relative to the *z*-axis was considered depending on the distance from the silica layer. Here, the OH bond vector points from the hydrogen atoms toward the oxygen of MeOH. The probability distribution $P(\cos\theta)$, where θ is the angle between the OH vector and the space-fixed *z*-axis, for the orientation of the MeOH molecule is shown in Figure 4. This analysis is done for three layers, each 5 Å wide. The first layer includes MeOH molecules within 5 Å of the silica-oxygen atom and the second layer those between 5 and 10 Å. The third layer contains

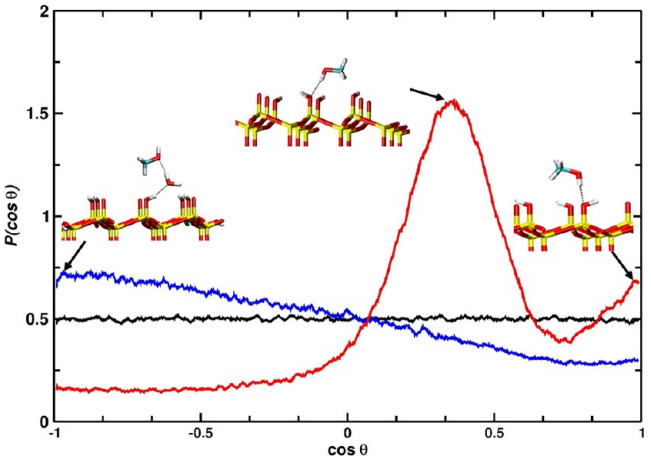

Figure 4. Average probability distribution for the MeOH −OH bond vector in different layers along the column, averaged over 1 ns. The orientation of the −OH bond vector within 5 Å of silica oxygen in red, in a layer from 5 to 10 Å (blue) and in the middle of the column (black). Structural representations for features in the probability distribution functions are also provided. The color scheme is carbon (blue), oxygen (red), silicium (yellow), and hydrogen (white).

methanol from the middle of the column between 35 and 40 Å. Figure 4 demonstrates that the −OH bond vector in the first layer has two preferred orientations (red line), while in the second layer (blue line) the −OH bond vector predominantly orients in an antiparallel fashion relative to the first-layer water molecules. The probability distribution for the −OH bond vector in the middle of the column is uniform as would be expected (black line).

Figures 5A,B show the time evolution of the phase thickness for C_{18} and C_{17}-phenyl derivatized alkyl chains and suggests that phase thickness depends upon the density of alkyl chains grafted on the silica surface and solvent composition. Table 2 establishes that for low surface coverage all functionalized chains collapse a behavior already observed in previous simulations.[10] At very low grafting density, the chain behaves much like an isolated chain in solution, since they have more spatial freedom; however, at high grafting density the polymer enters the "brush" regime, a theoretical observation made by Alexander[42] and de Gennes.[43] Because the chains are more densely packed and due to increased hydrophobic interactions among themselves, they have less freedom to move (rotate or bend). Another factor that influences the spatial extent of the chains is the increased amount of methanol in the mixture which was also observed with acetonitrile as a solvent (see Table 2 for comparison).[10] We also observed that chains with

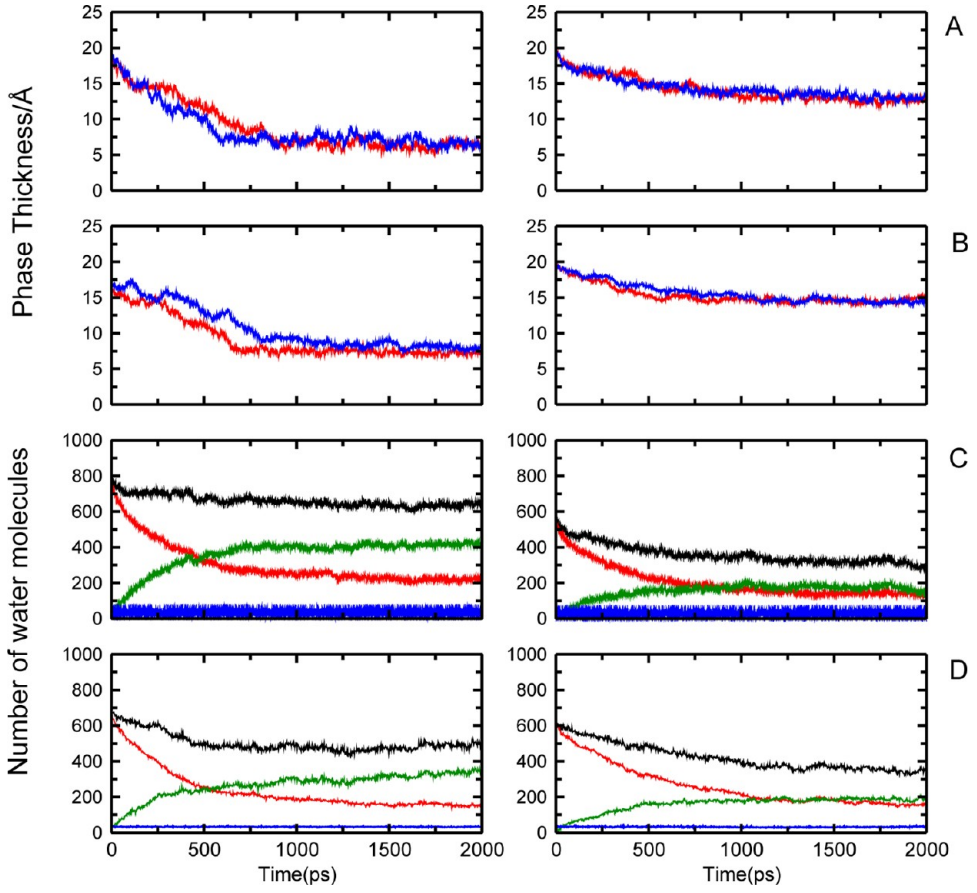

Figure 5. Temporal development of the phase thickness for unfunctionalized C_{18} (A) and C_{17}-phenyl (B) with W/MeOH compositions of 80/20 (red) and 50/50 (blue). Left column is for low surface coverage (0.88 μmol/m^2) and right column for high surface coverage (2.65 μmol/m^2). The solvent exchange dynamics in high surface coverage (2.65 μmol/m^2) C_{18} is reported in panels C and D. The left column is for 80/20 W/MeOH solvent mixture and the right column for 50/50 W/MeOH solvent mixture. Red traces represent outflow of water molecules from the stationary phase to the bulk phase; green, inflow of water molecules from the bulk to the stationary phase; black, total number of water molecules in the stationary phase (sum of red and green traces); blue, the occupation of the hydroxyl groups on the silica layers.

dx.doi.org/10.1021/jp305351f | J. Phys. Chem. B 2012, 116, 10951−10959

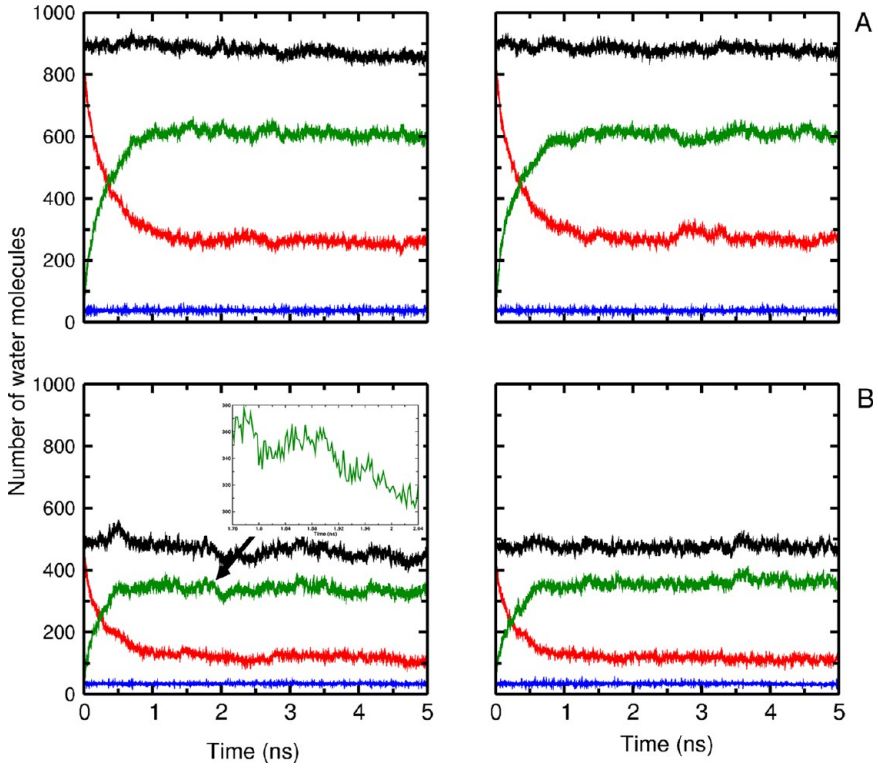

Figure 6. Inflow and outflow of water molecules from between the alkyl chains measured after introducing acridine orange into C_{17}-phenyl systems with high surface coverage and W/MeOH compositions of 100/0 (A) and 80/20 (B). Left column for protonated acridine (NH^+) and right column for the neutral state (N). The red trace represents outflow of water molecules from the stationary phase to the bulk; green, inflow of water molecules from the bulk to the stationary phase; black, total number of water molecules in the stationary phase (sum of red and green trace); blue, occupation of the hydroxyl groups on the silica layers.

polar terminal groups (−CN, $-NO_2$, $-NH_2$; see Figure S4 and Table 2) are more extended than with nonpolar functionalizations ($-C_{18}$, $-C_6H_5$). Polar termini provide a favorable environment for water or methanol molecules to interact, which may contribute to their more extended conformation. In comparing water/ACN and water/MeOH mixtures with the same organic volume fraction, more pronounced solvent penetration for ACN is found compared to MeOH which is consistent with previous work.[29] There is enrichment of the organic cosolvent in the interfacial region, and this effect is more pronounced for 80/20 compared to 50/50 solvent mixture and is more than the bulk density, as found from Monte Carlo simulations.[29] Similar behavior is found for the other derivatized surface $C_{17}-CN$, $C_{18}-NH_2$, $C_{18}-NO_2$ (see Figure S4).

C. Exchange Dynamics. For analyzing the water exchange dynamics between regions II and III, the water flux between these regions was determined. During the MD simulations the number of water molecules exchanged is reported in Figures 5C,D (for C_{18} and C_{17}-phenyl and high surface coverage). The analysis shows that water molecules initially in region II exchange with region III and vice versa. It is also found that systems with different W/MeOH ratios exhibit significantly different numbers of water in the stationary phase. The numbers of water molecules in region I directly interacting with the silica, i.e., are H-bonded to the Si−OH groups, are summarized in Table 2.

The number of water molecules in region I found here is similar to what was observed previously for acetonitrile as a solvent[38] and previous work with MeOH as a solvent.[29] The data in Table 2 show that as the volume fraction of organic modifier increases, the number of water molecules in H-bonding contact with the silica surface decreases. This is due to the presence of MeOH which competes for H-bonding to the surface −OH group. Depending on the systems, the numbers of water molecules that are exchanged between the regions are different. Figure 5C (left) reports results for a C18 column with a 80/20 solvent mixture. The red trace follows the number of waters exchanged (≈250) between regions II and III, compared to the initial state at $t = 0$. After less than 1 ns a steady state is reached. At the same time, the number of water molecules entering from region III to II is ≈450 (green), whereas the black trace reports the total number of water molecules always residing in region II, which is ≈700 during the entire simulation. For C18 and 50/50 solvent mixtures (Figure 5C (right) the amount of water pumped in and out between regions II and III is ≈200, similar to a 80/20 mixture, whereas the number of water molecules that exchange with region III is larger for 80/20 than that for a 50/50 solvent mixture. A similar behavior is observed for other functionalized chains (see Figure S4). Typically, reaching an equilibrium in the exchange dynamics is slower for 50/50 mixtures compared to 80/20. Quantitatively, all 80/20 systems are equilibrated in less than 1 ns, whereas it can take up to 1.5 ns for 50/50 mixtures. This is probably due to the increased number of water−MeOH hydrogen bonds in 50/50 compared to 80/20 mixtures.

D. Dynamics of Acridine Orange. In order to better characterize the consequences of different solvent composition and surface densities, the dynamics of an analyte molecule was followed. Acridine orange has been previously used to characterize interfacial dynamics at the stationary phase/solvent layer.[44−48] It was found that it can interact with the surface via

chemisorption or intercalation within these functionalized chains. For investigating the dynamics of acridine orange at the C_{17}-phenyl/solvent interface, acridine orange was introduced in the system 3 Å above the C_{17}-phenyl layer in different W/MeOH compositions (100/0, 80/20, 50/50). The exchange dynamics of water following the perturbation of the system is reported in Figure 6. With increasing MeOH concentration the number of exchanged water molecules decreases, and the time for equilibrating water exchange increases from ≈200 to 500 ps as shown in Figures 6A,B. With regards to solvent flow, all systems are well equilibrated on the 5 ns time scale. Occasionally, "avalanches" of solvent can be observed in which there is a sudden change in the number of water molecules; see inset Figure 6B, where the number of water molecules changes from 350 to 300 in region II (green line) in less than 1 ns.[38]

To characterize the motion of acridine orange relative to the surface, the *z*-coordinate of the acridine orange center-of-mass (COM) is reported as a function of time. Figure 7 suggests that the analyte molecule readily adsorbs to the C_{17}-phenyl interface, and due to the exchange of solvent and motion of the alkyl chains it moves in and out of the silica surface. Figures 7 A,B also suggest that there is no appreciable change in the average phase thickness (black curve) of the C_{17}-phenyl interface for all solvent compositions during 5 ns of MD simulation. For 100/0 W/MeOH solvent composition the analyte molecule is completely intercalated and remains there for the rest of the simulation. For other solvent mixtures (Figure 7B) the analyte molecule moves in and out of the stationary phase. For the simulation in C_{17}-phenyl with 100/0 solvent composition, the dynamics of acridine orange (NH^+) is shown in Figure 7C(I–IV). The snapshots are taken at different times along an MD simulation. These snapshots suggest that once the cavity at the surface is formed, the analyte molecule easily moves toward the surface and resides there for the rest of the simulation. The formation of a cavity is not directly observed in our simulations but results from the tendency of the alkyl chains to reduce the surface area by alkyl chain clustering, which in turn is enthalpy-driven as confirmed experimentally.[49] Clustering will lead to space on the silica surface which allows the analyte molecule to approach the surface and to intercalate. Cavity formation and intercalation of analyte molecules is an element of the slot model[50] and has been a matter of debate for the past few years.

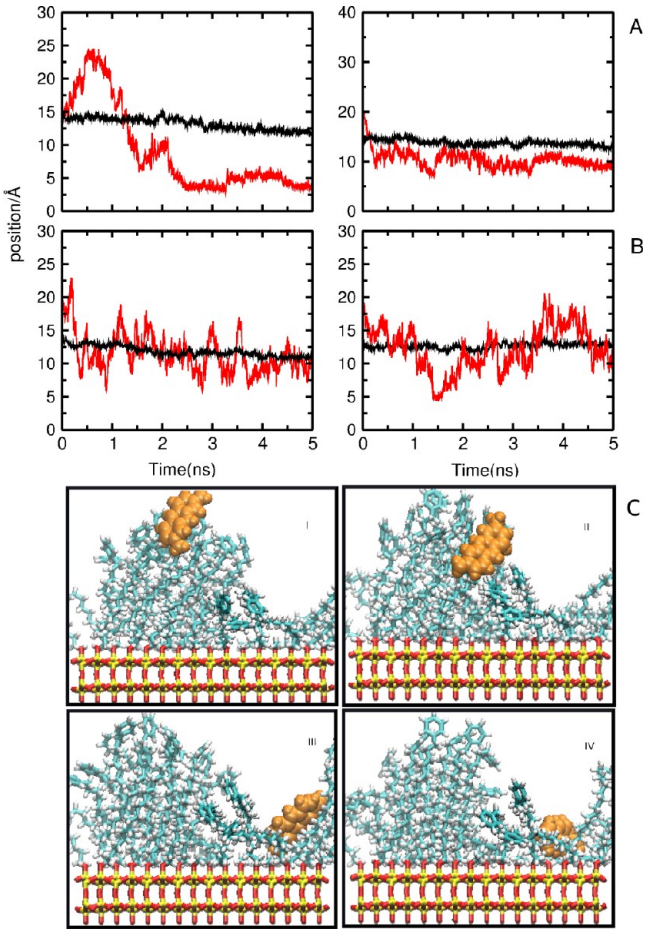

Figure 7. (A, B) The average height of the acridine center-of-mass above the silica layer (red trace) for protonated (left) and neutral (right) acridine orange in equilibrated, high-coverage C_{17}-phenyl. The solvent composition is 100/0 (A) and 80/20 (B) for W/MeOH. (C) Intercalation of acridine into the derivatized silica surface. Color code: yellow: silicon atom of the surface; red: oxygen atoms of the silanol group; light green: C_{17}-phenyl chains; orange: VdW representation of the analyte molecule.

The dynamics of acridine orange can also be characterized in terms of a diffusion coefficient *D* (see eq 1). For high coverage C_{17}-phenyl the diffusion coefficient *D* of acridine orange increases with increasing MeOH concentration from 0.013 to 0.042 (10^{-4} cm^2/s) in going from W/MeOH mixtures of 100/0 to 80/20 and reaches 0.054 (10^{-4} cm^2/s) in 50/50 W/MeOH for unprotonated acridine. For protonated acridine the diffusion coefficients depend less strongly on the solvent composition. They range from 0.058 to 0.076 (10^{-4} cm^2/s) for solvent compositions of 100/0 to 50/50, respectively. As the analyte molecule moves toward the interface, its diffusion slows down. This can be quantified by considering acridine orange in 100/0 W/MeOH at different *z*-positions above the surface. For positions 20, 10, and 2 Å above the surface, D = 0.064, 0.024, and 0.014 × 10^{-4} cm^2/s are found. Experimentally, the lateral diffusion coefficient in pure water was found to be 0.042 (10^{-4} cm^2/s) which considerably slows down to 0.0013 (10^{-4} cm^2/s) in C_{18} columns.[51] While the diffusion coefficient in pure water and the slowdown in the presence of a stationary phase are correctly captured, the effect of the interface is only a factor of ≈4 in the simulations, compared with at least an order of magnitude experimentally.

IV. DISCUSSION AND CONCLUSION

The present work reports all-atom simulations of water/methanol mixtures for realistic models for RPLC. The simulation setup consists of two silica layer separated by 80 Å with five different terminal groups ($-CH_3$, $C_{17}-CN$, $C_{18}-NH_2$, $C_{18}NO_2$, $C_{17}-C_6H_5$) tethered to them. The structure and dynamics of all these systems are investigated with two different solvent compositions W/MeOH (80/20 and 50/50). The coverage of the silica surface, low and high (0.88 and 2.65 $\mu mol/m^2$), corresponds to realistic experimental conditions. It is found that the presence of alkyl chains creates a hydrophobic environment which repels water molecules and leads to solvent depletion within the stationary phase. However, also with MeOH as the cosolvent, direct hydration of SiOH is found. This is reminiscent of the situation with ACN as the cosolvent.

Microheterogeneity of the solvent mixture is found for all functionalizations and may be an important driving force in

chromatographic systems. However, its degree depends on the functionalization and the surface coverage (density of alkyl chains). Different solvent compositions and changes in the terminal groups also affect the dynamics of alkyl chains which modifies the local environment including surface roughness and average phase thickness. Increasing the size of the terminal group (e.g., CH_3 to phenyl) increases the phase thickness, particularly for high surface coverage and solvent close to the surface. The entire system, including the stationary phase and the solvent surrounding it, is highly dynamical. This is best illustrated by the continuous exchange of water between the stationary and the bulk phase. The number of water exchanged also depends on solvent composition and functionalization. To compare atomistic simulations with concrete mechanistic proposals for the principles underlying RPLC, the motion of a probe molecule near the interface was considered in some detail. On a time scale of 5 ns acridine orange spontaneously approaches the surface and intercalates into the C_{17}-phenyl interface with pure water as the solvent. In this case the surface had a preformed cavity to which the probe molecule was able to bind. Such a behavior is reminiscent of the slot model which, however, is a phenomenological model.[52] Partial support for the slot model was obtained from earlier atomistic simulations in which, however, no explicit solvent was present.[3,4,50] The present work extends and supports these considerations insofar as binding of an analyte to a preformed cavity is readily observed also in the presence of explicit solvent. However, formation of such cavities is expected to occur on longer time scales. Thus, for more a comprehensive understanding and characterization of the atomistic details of analyte binding in chromatographic system considerably longer simulations are required. This is also evident from the observation that for other solvent compositions, which are more relevant in applications, the probe molecule remains close to the C_{17}-phenyl headgroup and moves in and out of these chains without actual insertion into the stationary phase. Intercalation of acridine is governed not only by the surface coverage, solvent composition, or the derivatized silica surface but also by dynamical elements such as the formation of cavities on the surface due to alkyl chain motions.

In conclusion, chromatographic systems are highly dynamical, heterogeneous systems. The retention properties depend in a complex fashion on solvent composition, headgroup functionalization, surface coverage, and less obvious properties, including solvent gradients at the interface, the degree of hydration of the silica surface, and most likely additional factors. Some of the insights gained so far from atomistic simulations support existing thermodynamic models put forward, including the slot model, the notion of hydrated silica surfaces, and the proposal of solvent waters exhibiting different bonding strengths to the surface depending on the layer they are in. A full understanding of retention and chemical selectivity will build on these insights and require further systematic studies.

■ ASSOCIATED CONTENT

Ⓢ Supporting Information

Figures S1−S4. This material is available free of charge via the Internet at http://pubs.acs.org.

■ AUTHOR INFORMATION

Notes

The authors declare no competing financial interest.

■ ACKNOWLEDGMENTS

This work has been supported by the Swiss National Science Foundation (Grant 200020-134954 and the NCCR MUST) which is gratefully acknowledged.

■ REFERENCES

(1) Klatte, S.; Beck, T. *J. Phys. Chem.* **1996**, *100*, 5931−5934.
(2) Mountain, R. D. *J. Phys. Chem. A* **1999**, *103*, 10744.
(3) Lippa, K. A.; Sander, L. C.; Mountain, R. D. *Anal. Chem.* **2005**, *77*, 7852.
(4) Lippa, K. A.; Sander, L. C.; Mountain, R. D. *Anal. Chem.* **2005**, *77*, 7862.
(5) Zhang, L.; Sun, L.; Siepmann, J. I.; Schure, M. R. *J. Chromatogr., A* **2005**, *1079*, 127.
(6) Zhang, L.; Rafferty, J. L.; Siepmann, J. I.; Chen, B.; Schure, M. R. *J. Chromatogr., A* **2006**, *1126*, 219−231.
(7) Rafferty, J. L.; Zhang, L.; Siepmann, J. I.; Schure, M. R. *Anal. Chem.* **2007**, *79*, 6551−6558.
(8) Fouqueau, A.; Meuwly, M.; Bemish, R. J. *J. Phys. Chem. B* **2007**, *111*, 10208−10216.
(9) Rafferty, J. L.; Siepmann, J. I.; Schure, M. R. *Anal. Chem.* **2008**, *80*, 6214−6221.
(10) Braun, J.; Fouqueau, A.; Meuwly, M.; Bemish, R. J. *Phys. Chem. Chem. Phys.* **2008**, *10*, 4765−4777.
(11) Melnikov, S. M.; Hoeltzel, A.; Seidel-Morgenstern, A.; Tallarek, U. *J. Phys. Chem. C* **2009**, *113*, 9230−9238.
(12) Rafferty, J. L.; Siepmann, J. I.; Schure, M. R.; Grushka, E.; Grinberg, N. *Adv. Chromatogr.* **2010**, *48*, 1−55.
(13) Rafferty, J. L.; Siepmann, J. I.; Schure, M. R. *J. Chromatogr., A* **2011**, *1218*, 2203−2213.
(14) Rafferty, J. L.; Siepmann, J. I.; Schure, M. R. *J. Chromatogr., A* **2012**, *1223*, 24−34.
(15) Eaton, G.; Pena-Nunez, A. S.; Symons, M. C. R. *J. Chem. Soc., Faraday Trans.* **1988**, *84*, 2181−2193.
(16) Venables, D. S.; Schmuttenmaer, C. A. *J. Chem. Phys.* **1988**, *108*, 4935−4944.
(17) Venables, D. S.; Schmuttenmaer, C. A. *J. Chem. Phys.* **2000**, *113*, 11222−11236.
(18) Rowlen, K. L.; Harris, J. M. *Anal. Chem.* **1991**, *63*, 964−969.
(19) Goldammer, E. V.; Hertz, H. G. *J. Phys. Chem.* **1970**, *74*, 3734−3755.
(20) Leiter, H.; Patil, K. J.; Hertz, H. G. *J. Solution Chem.* **1983**, *12*, 503−517.
(21) Dawson, E. D.; Wallen, S. L. *J. Am. Chem. Soc.* **2002**, *124*, 14210−14220.
(22) Kovacs, H.; Laaksonen, A. *J. Am. Chem. Soc.* **1991**, *113*, 5596−5605.
(23) Marcus, Y.; Migron, Y. *J. Phys. Chem.* **1991**, *95*, 400−406.
(24) Woods, K. N.; Wiedemann, H. *J. Chem. Phys.* **2005**, *123*, 134507.
(25) Shulgin, I. L.; Ruckenstein, E. *Phys. Chem. Chem. Phys.* **2008**, *10*, 1097−1105.
(26) Bako, I.; Megyes, T.; Balint, S.; Grosz, T.; Chihaia, V. *Phys. Chem. Chem. Phys.* **2008**, *10*, 5004−5011.
(27) Reimers, J. R.; Hall, L. E. *J. Am. Chem. Soc.* **1999**, *121*, 3730−3744.
(28) Gritti, F.; Guiochon, G. *J. Chromatogr., A* **2006**, *1103*, 69−82.
(29) Rafferty, J. L.; Siepmann, J. I.; Schure, M. R. *J. Chromatogr., A* **2011**, *1218*, 2203−2213.
(30) Jorgensen, W. L.; Chandrasekhar, J.; Madura, J. D.; Impey, R. W.; Klein, C. L. *J. Chem. Phys.* **1983**, *79*, 926−935.
(31) MacKerell, A. D., Jr.; et al. *J. Phys. Chem. B* **1998**, *102*, 3586−3616.
(32) Ryckaert, J. P.; Ciccotti, G.; Berendsen, H. J. *J. Comput. Phys.* **1977**, *23*, 327−341.
(33) Price, M. L. P.; Ostrovsky, D.; Jorgensen, W. L. *J. Comput. Chem.* **2001**, *22*, 1340−1352.

(34) Brooks, B. R.; Bruccoleri, R. E.; Olafson, B. D.; States, D. J.; Swaminathan, S.; Karplus, M. *J. Comput. Chem.* **1983**, *4*, 187−217.
(35) Brooks, B. R.; et al. *J. Comput. Chem.* **2009**, *30*, 1545−1614.
(36) Allen, M. P.; Tildesley, D. J. *Computer Simulations of Liquids*, 3rd ed.; Oxford Science Publications: New York, 1987.
(37) Scott, R. P. W. *Faraday Symp. Chem. Soc.* **1980**, *15*, 49−68.
(38) Orzechowski, M.; Meuwly, M. *J. Phys. Chem. B* **2010**, *114*, 12203−12212.
(39) Dixit, S.; Crain, J.; Poon, W.; Finney, J.; Soper, A. *Nature* **2002**, *416*, 829−832.
(40) Dougan, L.; Bates, S.; Hargreaves, R.; Fox, J.; Crain, J.; Finney, J.; Reat, V.; Soper, A. *J. Chem. Phys.* **2004**, *121*, 6456−6462.
(41) Chou, S. G.; Soper, A. K.; Khodadadi, S.; Curtis, J. E.; Krueger, S.; Cicerone, M. T.; Fitch, A. N.; Shalaev, E. Y. *J. Phys. Chem. B* **2012**, *116*, 4439−4447.
(42) Alexander, S. *J. Phys. (Paris)* **1977**, *38*, 983.
(43) de Gennes, P. G. *Adv. Colloid Interface Sci.* **1987**, *27*, 189.
(44) Burbage, J. D.; Wirth, M. J. *J. Phys. Chem.* **1992**, *96*, 5943−5948.
(45) Burbage, J. D.; Wirth, M. J. *J. Phys. Chem.* **1992**, *96*, 9022−9025.
(46) Kovaleski, J. M.; Wirth, M. J. *J. Phys. Chem.* **1995**, *99*, 4091−4095.
(47) Kovaleski, J. M.; Wirth, M. J. *J. Phys. Chem.* **1996**, *100*, 10304−10309.
(48) Kovaleski, J. M.; Wirth, M. J. *J. Phys. Chem. B* **1997**, *101*, 5545−5548.
(49) Daumantas, M.; Bloomfield, V. A. *Biophys. Chem.* **2001**, *93*, 53.
(50) Lippa, K. A.; Sander, L. C. *J. Chromatogr., A* **2006**, *1128*, 79−89.
(51) Zulli, S. L.; Kovaleski, J. M.; Zhu, Z. R.; Harris, J. M.; Wirth, M. J. *Anal. Chem.* **1994**, *66*, 1708−1712.
(52) Wise, S. A.; Sander, L. C. *HRC & CC, J. High Resolut. Chromatogr. Chromatogr. Commun.* **1985**, *8*, 248.